

# Extraordinary high dielectric constant, electrical and magnetic properties of ferrite nanoparticles at room temperature

Khalid Mujasam Batoo · Feroz Ahmed Mir ·  
M.-S. Abd El-sadek · Md. Shahabuddin ·  
Niyaz Ahmed

Received: 5 March 2013 / Accepted: 9 October 2013 / Published online: 31 October 2013  
© Springer Science+Business Media Dordrecht 2013

**Abstract** Nanoparticles of spinel ferrites of basic composition  $\text{Ni}_{1-x}\text{Co}_x\text{Fe}_2\text{O}_4$  ( $0.0 \leq x \leq 0.05$ ) were synthesized through modified co-precipitation method, and were characterized for structural, transport electrical and magnetic properties using XRD, HRTEM, FTIR, LCR meter and VSM techniques, respectively. XRD analysis showed that all the samples are single-phase cubic spinel in structure. The average crystallite sizes of the nanoparticles were found between 30 nm to 45 nm. Real and imaginary parts of the impedance ( $Z'$  and  $Z''$ ) suggested coexistence of two relaxation regimes: one was introduced by electrode polarization, while the other was attributed to the coefficient of grain and grain boundary effects. The dielectric constant of the samples was found very high, which showed non-Debye relaxation

phenomena, while conductivity of the samples exhibited a two-segment behavior with frequency. The room temperature M–H curves suggested that the samples exhibit supermagnetism, and the saturation magnetization increases with increasing  $\text{Co}^{2+}$  ion substitution.

**Keywords** Nanoparticles · Ferrites · Impedance spectroscopy · Conductivity · Dielectric constant · Magnetization

## Introduction

Spinel ferrite nanoparticles (NPs) by virtue of their unique electronic, magnetic, and physical structure are an important class of materials because of their high resistivity and low eddy current losses (Son et al. 2002; Sugimoto 1999; Atif and Hasanian 2006). They find wide use in ultrahigh frequency applications. As NPs, they are also considered for biomedical applications, including as contrast agents in magnetic resonance imaging (Mitchell 1997), and in promising cancer remediation therapies such as target drug delivery, magnetohyperthermia, and magnetorheological fluids (Hafeli et al. 1997). However, the electromagnetic properties of ferrite NPs have been found to vary widely over the size, and with foreign element substitution (Hochepped et al. 2000; Morrison et al. 2004). In order to realize their full potential, understanding of processing

---

K. M. Batoo (✉)  
King Abdullah Institute for Nanotechnology, King Saud University, P.O. Box 2455, Riyadh 11451, Saudi Arabia  
e-mail: khalid.mujasam@gmail.com; kbatoo@ksu.edu.sa

F. A. Mir  
University Science Instrumentation Centre, University of Kashmir, Srinagar 190006, India

M.-S. Abd El-sadek  
Nanomaterial Laboratory, Physics Department, Faculty of Science, South Valley University, Qena 83523, Egypt

Md. Shahabuddin · N. Ahmed  
Department of Physics and Astronomy, King Saud University, P.O. Box 2455, Riyadh 11451, Saudi Arabia

and refinement of ferrite NPs is essential. One of the parameters of great importance is dielectric constant/dielectric loss which is very sensitive to cation–anion–cation bond angles, cation type and its valence state. Demonstrating its importance is an application of ferrite NPs in microwave devices, multilayer inductor chips, transformer cores, etc.

Nanocrystalline ferrite systems usually have a mixed spinel structure having chemical formula  $(M_{1-\delta}^{2+}Fe_{\delta}^{3+})[M_{\delta}^{2+}Fe_{\delta}^{2-}]O_4^{2-}$ . The divalent metal ion  $M^{2+}$  can occupy either tetrahedral (A) or octahedral [B] sites or both sites of a spinel structure, depending upon the nature of a system. The inversion parameter,  $\delta$ , is defined as the fraction of (A) sites occupied by  $Fe^{3+}$  cations and its value depends on method of preparation (Willard et al. 2004; Tug et al. 2002).  $NiFe_2O_4$  is one of the most important magnetic materials, and therefore, is extensively used in high frequency applications via microwave devices due to their high resistivity and low dielectric losses. It is reported (Chinnasamy et al. 2001) that nanocrystalline  $NiFe_2O_4$  exhibits a mixed spinel structure with  $Ni^{2+}$  ions occupying both (A) and [B] sites.  $NiFe_2O_4$  NPs with a mixed spinel structure have been shown to exhibit interesting electrical, magnetic, gas, and humidity sensing properties (Morrison et al. 2004; Jacob and Khadar 2010; Brook and Kingery 1967).

In order to differentiate between transport characteristic such as grain and grain boundary in ferrites, impedance spectroscopy (IS) is one of the powerful techniques to carry out (Macdonald 1987). The microstructure of ferrites comprises two main components; grain and grain boundary, and the correspondence between the two is important to understand the overall properties of these materials (Idrees et al. 2010). IS can be employed to investigate the conduction mechanism in different microstructures (phases) inside a polycrystalline material. By using impedance technique, real and imaginary parts of complex electrical quantities are measured as a function of frequency of the applied field (Barsoukov and Macdonald 2005). These complex quantities include electrical impedance, dielectric permittivity, and loss tangent. The grain boundaries are found to have main control over the electrical properties of ferrites (Gopalan et al. 2008). The study of dielectric and impedance properties of  $NiFe_2O_4$  NPs will be constructive for extensive range of applications.

In this paper, we present a detailed report on synthesis of Co-doped  $Ni_{1-x}Co_xFe_2O_4$  ferrite NPs and study of their structural, dielectric, impedance, and magnetic properties to determine any possible change in the conduction or magnetic properties due to substitution effect.

## Experimental method

### Material preparation

The raw materials used to synthesize NPs of  $Ni_{1-x}Co_xFe_2O_4$  (where  $x = 0.0, 0.1, 0.2, 0.3, 0.4$  and  $0.5$ ) were nickel chloride (99 % Merck, India), cobalt (III) chloride (99 % Merck, India), iron (III) chloride (98 % Merck, India), and sodium hydroxide (98 % Merck, India). The weighted amounts of the chlorides were dissolved in a mixture of 50 ml double distilled and 25 ml ethanol. The mixed metal chloride precursor solution was introduced slowly into a boiling 1 M NaOH solution, and the reaction was carried out at 98 °C for 120 min. The pH value of solution was fixed at 7. The pH environment is critical to particle nucleation, rate of growth, stabilization and ultimately size of the resulting particles. Following the completion of reaction, resulting particles were rinsed in distilled water, filtered, and dried at 70 °C for 36 h.

### Characterization techniques

The structural characterizations of grown samples were performed by an X-ray diffractometer (XRD, PANalytical X'Pert Pro X-ray diffractometer) with CuK $\alpha$  radiation ( $\lambda = 1.5418 \text{ \AA}$ ). The intensities were recorded for 20°–80° with a step scan of 0.02° min<sup>-1</sup>. For morphological studies, high-resolution transmission electron microscopy (HRTEM, Jeol 2010, JEOL USA, Inc.) was performed. Fourier inferred spectroscopy (FT-IR, Nicolet Instrument Corp.) measurements were carried out in the range of 400–4000 cm<sup>-1</sup>. For dielectric and impedance measurements, powder samples were pressed into circular disk-shaped pellets, and silver paste coating was done on the opposite faces of pellets in order to make parallel pellet capacitor geometry with ferrite material as dielectric medium. The dielectric and impedance measurements were

carried out between 42 Hz to 5 MHz using LCR HI-Tester (HIOKI 3532-50) at room temperature. Room temperature magnetic hysteresis was measured by Microsense VSM (model EV9) measurement setup.

## Results and discussion

### Structural and morphological analysis

Figure 1 shows the X-ray diffraction pattern of  $Ni_{1-x}Co_xFe_2O_4$  ferrite NPs, which confirms single-phase cubic spinel structure of samples excluding signature of any secondary phase corresponding to any structure. The average crystallite size of grown NPs was determined using Scherer's formula (Battoo and Ansari 2012):

$$t = \frac{k\lambda}{\beta \cos\theta}, \tag{1}$$

where  $t$  is the crystallite size,  $\beta$  is the full width at half maximum of the peak (311), and  $k$  is an instrumental constant. The average crystallite size was found between 30 nm to 45 nm. The lattice parameter of the samples was calculated using the formula:

$$a = \frac{(h^2 + k^2 + l^2)^{1/2}}{2\sin\theta}, \tag{2}$$

The lattice parameter of the samples was found between 8.48 and 8.57 Å, tabulated in Table 1. The lattice parameter of undoped sample is less than that

reported for bulk  $NiFe_2O_4$  (Phadataré et al. 2012). The reduction in lattice parameter may be attributed to the increased degree of inversion, more surface energy, and surface tension which leads to the reduction of lattice constant (Atif and Hasanian 2006; Lee et al. 2007). The increase in lattice parameter with increasing doping concentration is attributed to the mismatch of ionic radii where smaller ionic radii  $Ni^{2+}$  (0.64 Å) are replaced by larger ionic radii  $Co^{2+}$  (0.65 Å), and hence the lattice parameter increases (Phadataré et al. 2012; Ata-Allah and Kaiser 2004).

Figure 2 presents the HRTEM micrographs with inset showing average grain size distribution and selective area electron diffraction (SAED) pattern for the compositions  $x = 0.0$  and 0.1, respectively. The average sizes of crystallites were found between 30 nm to 45 nm. The NPs were found highly agglomerated with less uniformity in size. The agglomeration of NPs can be because they experience a permanent magnetic moment proportional to their volume (Suryawanshi et al. 1999). In the SAED pattern, distinct diffuse rings are observed that confirm high crystalline order of the samples. The crystallographic  $d$  value of 2.512 Å corresponding to the lattice space of (311) was observed, which corroborates well with that obtained from XRD analysis.

### FT-IR

The room temperature FT-IR spectra of the  $Ni_{1-x}Co_xFe_2O_4$  ferrite NPs are shown in Fig. 3. The spectra were recorded in the range of 400–4,000  $cm^{-1}$ . The absorption band observed around 1,115  $cm^{-1}$  is assigned to C–O–H, while the bands observed at 1,636 and 3,453  $cm^{-1}$  are assigned to O–H group. The IR absorption bands of solids observed in the range of 100–1,000  $cm^{-1}$  are usually assigned to vibrations of ions in the crystal lattice (Waldron 1955; Wilson and Wells 1946). In case of ferrites, generally two absorption bands appear, one around 600  $cm^{-1}$ :  $\nu_1$ , which is attributed to the stretching vibration of tetrahedral group Fe–O and the second around 400  $cm^{-1}$ :  $\nu_2$ , which is attributed to the octahedral group complex Fe–O. From IR spectra, it is noted that no shift occurs in band positions,  $\nu_1$  and  $\nu_2$ , by increasing Co content (Table 1). It is seen that the intensity of bands increases while broadening remains same, which shows that the samples are more ordered (Ata-Allah and Kaiser 2004).

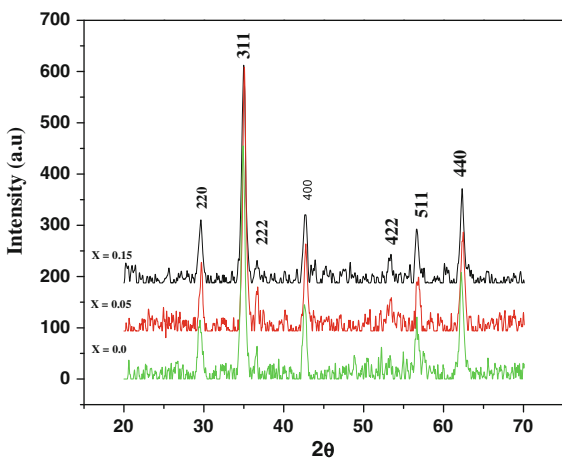
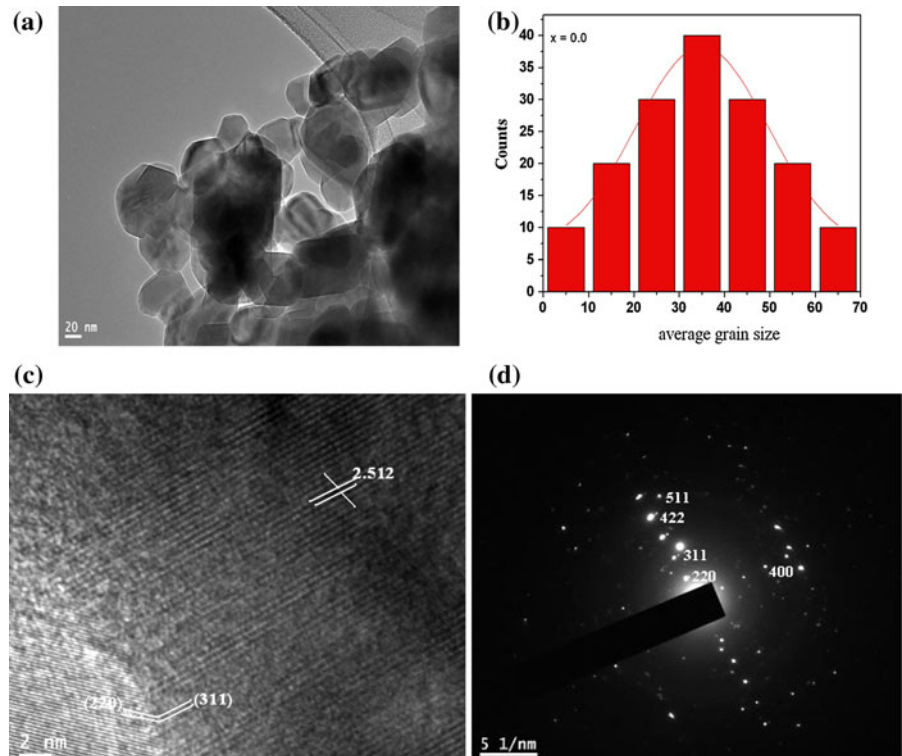


**Fig. 1** The XRD pattern of the  $Ni_{1-x}Co_xFe_2O_4$  ferrite nanoparticles

**Table 1** Grain size, lattice parameters, and FT-IR spectra data of Ni<sub>1-x</sub>Co<sub>x</sub>Fe<sub>2</sub>O<sub>4</sub> ferrite nanoparticles

Composition (x)	Crystallite size (nm (±1))	Lattice parameter (Å)	$\nu_1$ (cm <sup>-1</sup> )	$\nu_2$ (cm <sup>-1</sup> )	$M_s$ (emu/g)
0.0	30	8.48	602.9	414.6	23.19
0.1	35	8.50	602.9	414.6	33.18
0.2	38	8.52	602.9	414.6	38.70
0.3	40	8.53	602.9	414.6	43.97
0.4	45	8.56	602.9	414.6	44.20

**Fig. 2** **a** TEM micrograph. **b** Grain size distribution. **c** Lattice planes, and **d** SAED pattern for composition  $x = 0.0$



Impedance spectroscopy (IS)

Figure 4a, b shows the variation of real and imaginary parts of impedance ( $Z'$  and  $Z''$ , respectively) with the frequency between 42 Hz–5 MHz at room temperature. The real and imaginary parts of impedance were calculated according to the following equations (Macdonald 1987; Suryavanshi et al. 1991; Arcos et al. 1999):

$$Z' = \frac{R_g}{1 + \omega_g^2 C_g^2 R_g^2} + \frac{R_{gb}}{1 + \omega_{gb}^2 C_{gb}^2 R_{gb}^2}, \tag{4}$$

$$Z'' = \frac{-R_g^2 C_g \omega_g}{1 + \omega_g^2 C_g^2 R_g^2} + \frac{-R_{gb}^2 C_{gb} \omega_{gb}}{1 + \omega_{gb}^2 C_{gb}^2 R_{gb}^2}, \tag{5}$$

where the terms  $R_g$  and  $C_g$  represents the resistance and the capacitance of grain, while  $R_{gb}$  and  $C_{gb}$  represent the corresponding terms for grain boundary volume. The resistance values for grain and grain boundary have been calculated from the intercepts on real part of  $Z$  ( $Z'$ ) axis, whereas the capacitance values have been calculated from the frequency peaks of semicircle arc. Since the value of  $Z' = -Z''$  at maximum, we have (Macdonald 1992; Arcos et al. 1999; Zaki and Mansour 2006):

$$C_g = \frac{1}{R_g \omega_g}, \tag{6}$$

$$C_{gb} = \frac{1}{R_{gb} \omega_{gb}}, \tag{7}$$

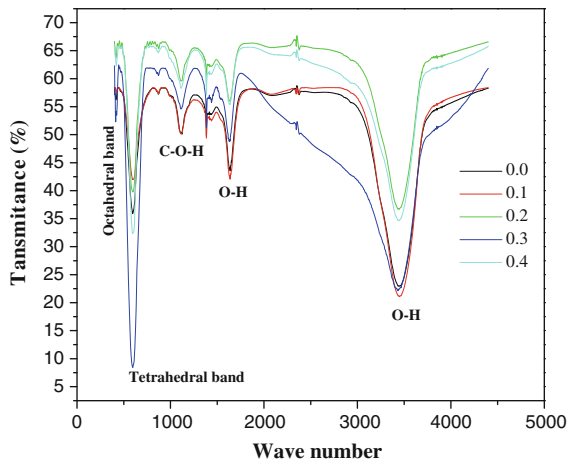


**Fig. 3** The FTIR spectra for  $Ni_{1-x}Co_xFe_2O_4$  ferrite nanoparticles

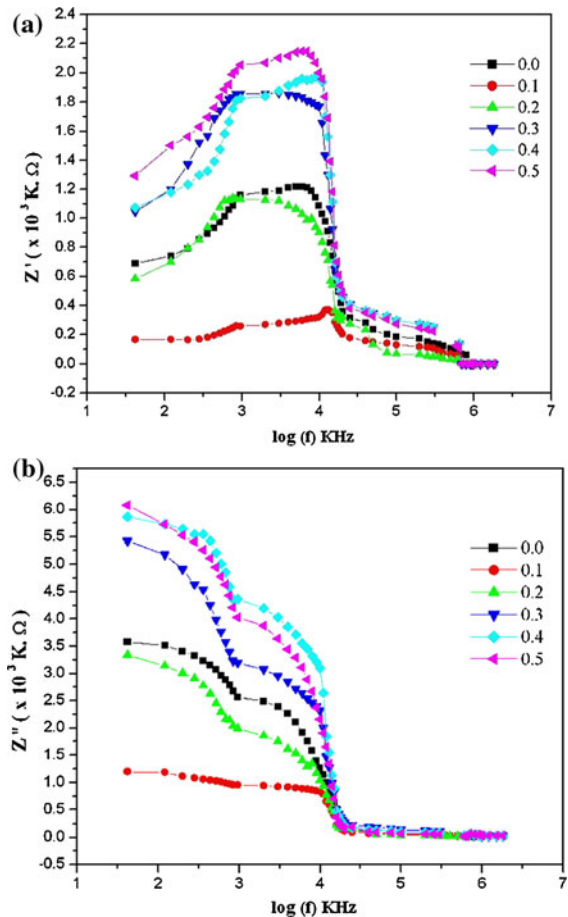


**Fig. 4** a, b The variation of  $Z'$  and  $Z''$  with frequency for  $Ni_{1-x}Co_xFe_2O_4$  ferrite nanoparticles

A frequency dependent  $Z'$  plateau is observed initially in low frequency side followed by a nearly positive slope at high frequency side, indicating a crossover from low frequency relaxation behavior to high frequency dispersion phenomenon. It is seen that  $Z'$  value decreases rapidly above 12 kHz with increasing value of frequency. Figure 4b shows a broad imaginary impedance peak ( $Z''$ ) which moves to high frequency side (step like) with little negative slope and finally disappears above 12 kHz and becomes almost frequency independent. The observed decrease in both  $Z'$  and  $Z''$  can be attributed to the increase in conduction mechanism due to hopping of electrons, which increases with increasing frequency of the applied field (Bauerle 1969; Srivastava et al. 2009; Ortega et al. 2008).

Nyquist plots for various compositions of  $Ni_{1-x}Co_xFe_2O_4$  ferrite NPs in the frequency range of 42 Hz–5 MHz at room temperature are presented in Fig. 5. It is seen that each sample exhibits almost a complete semicircle arc, and the radius of semicircle gradually increases with increasing doping concentration except for 10 % doping where it decreases. The lower total resistance at this composition promotes electron hopping, which is known to be mechanism for both conduction and polarization in ferrites. The grain boundary resistances are larger than grain resistances. This is ascribed to the fact that atomic arrangement near

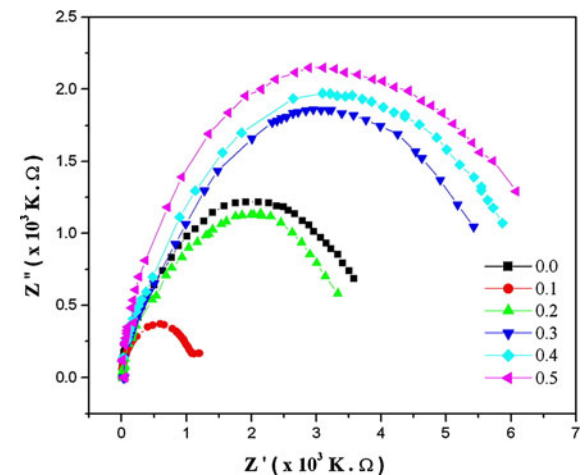


**Fig. 5** The variation of  $Z''$  versus  $Z'$  for  $Ni_{1-x}Co_xFe_2O_4$  ferrite nanoparticles

grain boundary region is disordered, which increases electron scattering (Dutta et al. 2004). It can be seen that none of the composition exhibit two semicircles corresponding to the grain and grain boundary in Cole–Cole plot, except for  $x = 0.1$ , which shows emergence of one more semicircle at low frequency region. The second semicircle may be attributed to the electrode polarization. Therefore, we propose that the semicircles corresponding to the grain and grains boundaries overlap and their individual effects cannot be separately evaluated due to sufficiently high grain boundary resistance values, which increase drastically with the progressive increment in doping concentration contrary to the grain resistance values.

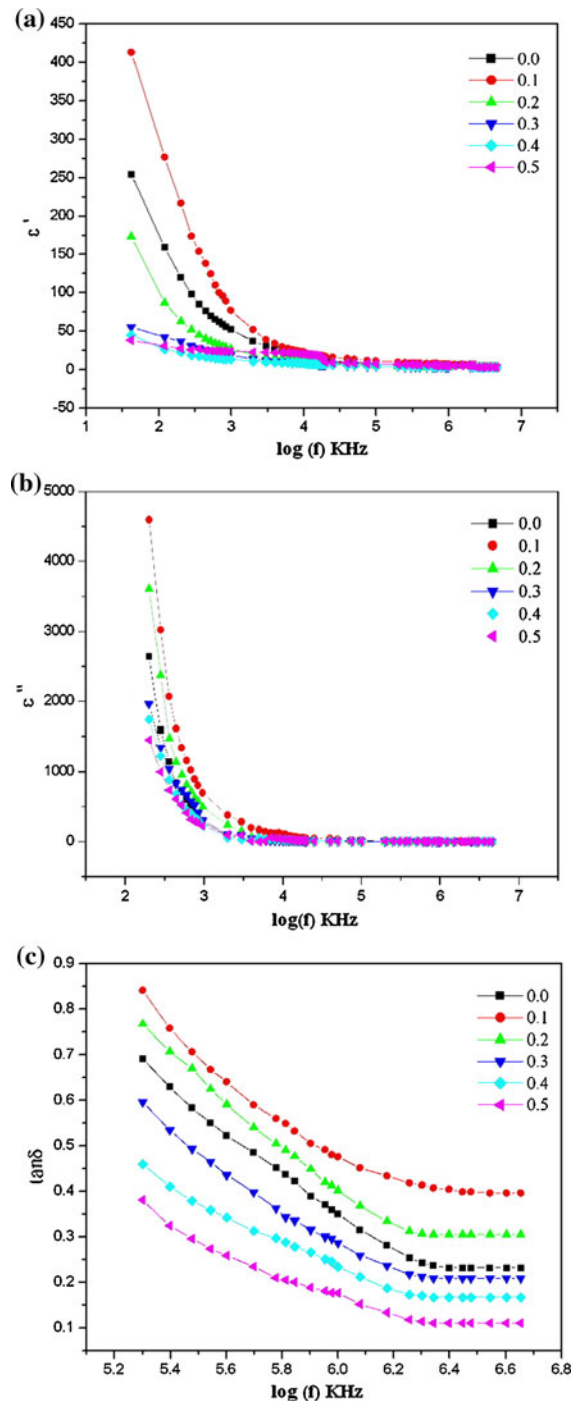
### Dielectric properties

Figure 6a–c shows real, imaginary part of the dielectric constant, and dielectric loss ( $\epsilon'$ ,  $\epsilon''$ , and  $\tan\delta$ ) plotted against frequency at room temperature. It is seen that all the dielectric parameters ( $\epsilon'$ ,  $\epsilon''$ , and  $\tan\delta$ ) show a strong dispersion with increasing value of frequency and the response becomes almost frequency independent for real and imaginary parts of the dielectric constant at higher frequency, while  $\tan\delta$  continuously decreases with increasing value of frequency. The dielectric constant of the samples is found exceptionally high while loss factor has been found less than 1 which makes present material as good choice for high frequency/microwave applications. Further, it is seen that no relaxation or Debye peaks are observed in any composition for both real and imaginary parts of dielectric constant, but a weak relaxation phenomenon is noticed in dielectric loss for the compositions,  $x = 0.4$  and  $0.5$ , respectively. The observed relaxation behavior can be attributed to the ferromagnetic resonance where matching of electron hopping frequency and the frequency of applied field (Chen et al. 2010) happens.

### Ac conductivity

Real conductivity is usually adopted for studying ion motion in ionic oxides or gases. The real conduction in present study has been calculated using Eq. (Abbas et al. 2007):

$$\sigma' = \frac{d \cos \theta}{A|Z|}, \quad (8)$$



**Fig. 6** a–c The real, imaginary part of the dielectric constant, and dielectric loss ( $\epsilon'$ ,  $\epsilon''$  and  $\tan\delta$ ) versus frequency for  $\text{Ni}_{1-x}\text{Co}_x\text{Fe}_2\text{O}_4$  ferrite nanoparticles

where  $d$  is the sample thickness,  $A$  is top electrode area,  $\theta$  is impedance phase angle, and  $|Z|$  is absolute impedance value. The real conductivity spectra are

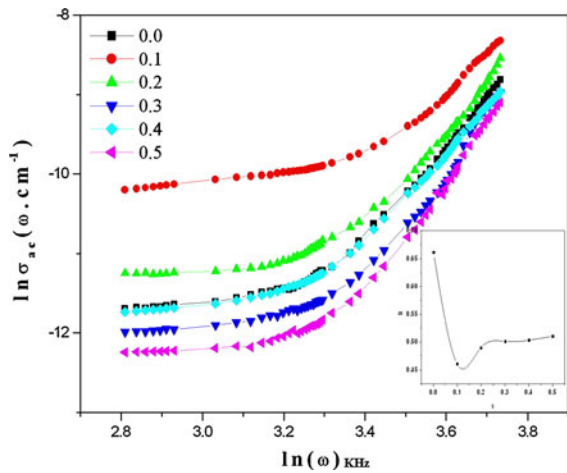


**Fig. 7** The variation of ac conductivity with frequency with *inset* showing variation of exponent with composition for  $Ni_{1-x}Co_xFe_2O_4$  ferrite nanoparticles

hence presented in Fig. 7 as a function of frequency (42 Hz–5 MHz) at room temperature. It may be seen that at high frequency, the conductivity increases exponentially and moves to higher side of frequency window. According to jumping relaxation model (Abbas et al. 2007; Patange et al. 2009), at low frequencies, where the conductivity is constant, transport takes place on infinite paths (dc conductivity). The conductivity in low frequency region is associated with the successful hops to its neighborhood vacant site due to available long time period; such successive jumps result in a long-range transitional motion of ions contributing to dc conductivity. At higher frequencies, the conductivity increases strongly with frequency. The electrical transport phenomenon is dominated by contributions from hopping between infinite clusters (ac conductivity). Two competing relaxation processes can be realized at

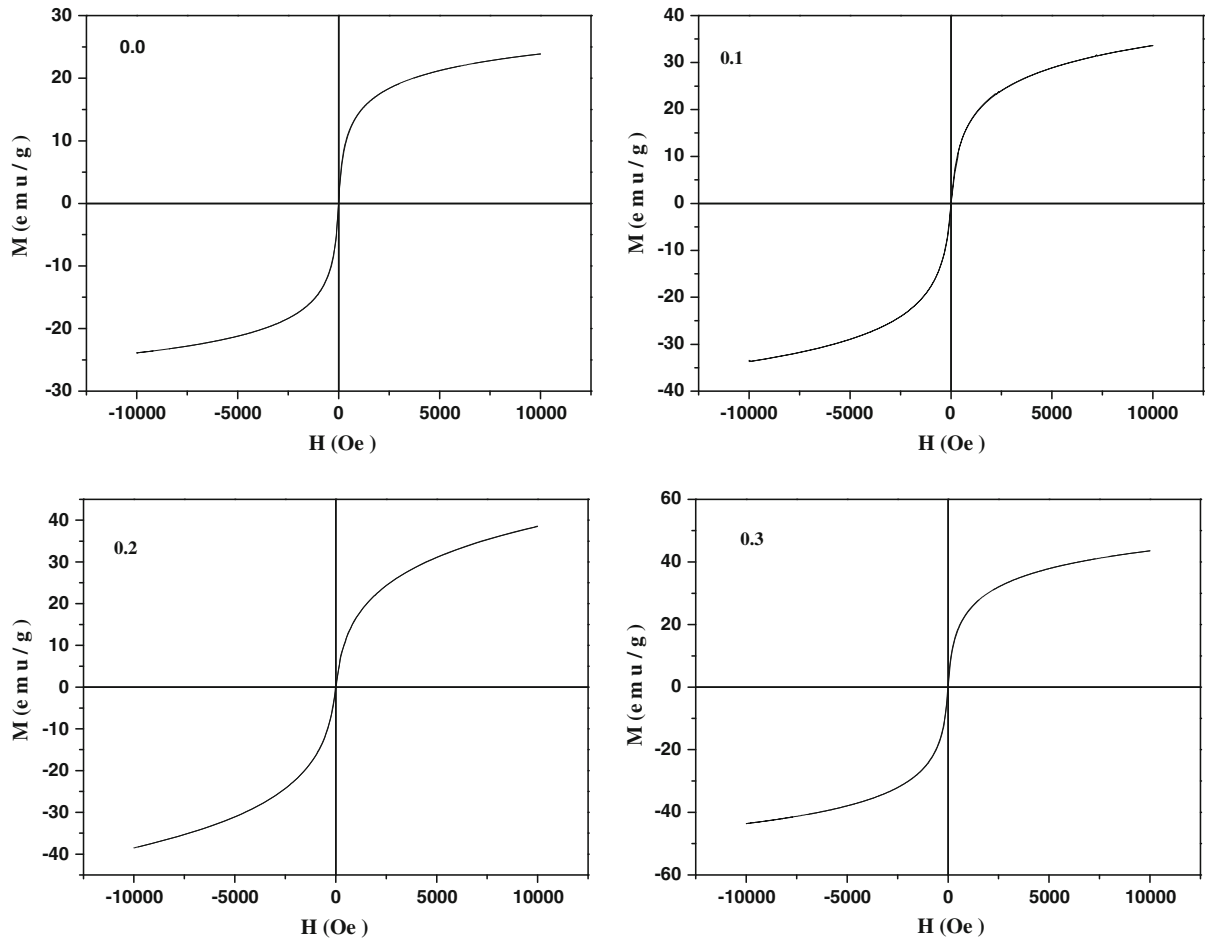


**Fig. 8** Room temperature hysteresis for  $Ni_{1-x}Co_xFe_2O_4$  ferrite nanoparticles

this stage which can be termed as unsuccessful, i.e., when jumping ion jumps back to initial position, and successful, i.e., when neighborhood ions become relaxed with respect to ions position. The increase in ratio of successful to unsuccessful ion hopping results in more dispersive conductivity at higher frequencies as observed in present study (Abbas et al. 2007).

The exponent ‘ $n$ ’ has been calculated as a function of composition by plotting  $\ln \sigma$  versus  $\ln \omega$  according using Eq. (5), which represents straight line with slope equal to the exponent ‘ $n$ ’ and intercept equal to  $\ln B$  on vertical axis at  $\ln \omega = 0$ .

$$\sigma_{ac}(\omega, T) = B\omega^n, \quad (9)$$

where constants  $B$  and  $n$  are composition and temperature dependent parameters. The inset in Fig. 8 shows the variation of ‘ $n$ ’ as a function of  $\text{Co}^{2+}$  ion doping. In present study, value of parameter  $n$  has been found between 0.104 and 0.177, which corresponds to short range transitional hopping of charges or ac conductivity (Bauerle 1969).

### Magnetic properties

Figure 8 shows the hysteresis loops for first four grown ferrite nanoparticle samples at room temperature. Interestingly, from the hysteresis loops, it is seen that the coercivity and the remanence magnetization are zero for all samples. The samples are not saturated even with the applied magnetic field of 10 KOe, which show the characteristics of superparamagnetism (Ghasemi et al. 2012). The variation of magnetization of ferrite NPs show that up to a specific magnetic field, magnetic moments of core align with the applied field and beyond this field; any increase in the applied field has an effect on the shell of particles, and therefore, the slope of magnetization decreases with increasing applied field (Abbas et al. 2007). Further, from Fig. 8 it is noted that the magnetization increases with increasing doping concentration of  $\text{Co}^{2+}$  ions. This increase in magnetization is due to replacement of  $\text{Co}^{2+}$  ions of magnetic moment  $2 \mu_B$  with lower magnetic moment  $1 \mu_B$  cations such as  $\text{Ni}^{2+}$  ions. A systematic change in the shape of virgin curve is observed, which shows transition from a pinning type magnet in case of pure  $\text{NiFe}_2\text{O}_4$  ferrite due to a large spin disordering (Kodama et al. 1996). The tendency for softening and transition to a nucleation type magnetic is seen in the increasing steepness of virgin

curves with increasing doping concentration and becomes maximum for  $x = 0.4$  (not shown in graph). Also, this increased value of saturation magnetization can be due to partial replacement of  $\text{Fe}^{3+}$  ions with  $\text{Co}^{3+}$  ions (Ghasemi et al. 2012; Thakur et al. 2012).

### Conclusion

Single phase, high crystalline ordered  $\text{Ni}_{1-x}\text{Co}_x\text{Fe}_2\text{O}_4$  ferrite NPs were synthesized through modified citrate-gel method. The dielectric properties show a non-Debye relaxation mechanism, with 10 % doping having maximum value of dielectric constant. The dielectric loss has been found less than 1 in the grown NPs, which makes synthesized material a good choice for high frequency applications. The hysteresis curves of samples show that the grown ferrite NPs exhibit superparamagnetism. The saturation magnetization was found to increase with progressive substitution of  $\text{Co}^{2+}$  ions.

**Acknowledgments** K.M. Batoo is thankful to the National Plan for Science and Technology (NPST), King Saud University for providing the financial support under the project code: 10NAN1999-02 for carrying this work.

### References

- Abbas SM, Chatterjee R, Dixit AK, Kumar AVR, Goel TC (2007) Electromagnetic and microwave absorption properties of ( $\text{Co}^{2+}$ - $\text{Si}^{4+}$ ) substituted barium hexaferrites and its polymer composite. *J Appl Phys* 101:074105–074111
- Arcos D, Vazquez M, Valenzuela M, Regi MV (1999) Grain boundary impedance of doped Mn–Zn ferrites. *J Mater Res* 3:861–865
- Ata-Allah SS, Kaiser M (2004) Semiconductor-to-metallic transition in Cu-substituted Ni–Mn ferrite. *Phys Stat Sol* 201:3157–3165
- Atif M, Hasanian SK (2006) Magnetization of sol–gel prepared Zinc ferrite nanoparticles: effects of inversion and particle size. *Sol State Commun* 138:416–421
- Barsoukov E, Macdonald JR (2005) Impedance spectroscopy theory, experiments and applications. Wiley, New York
- Batoo KM, Ansari MS (2012) Low temperature-fired Ni–Cu–Zn ferrite nanoparticles through auto-combustion method for multilayer chip inductor applications. *Nanoscale Res Lett* 7:1–14
- Bauerle E (1969) Study of solid electrolyte polarization by a complex admittance method. *J Phys Chem Sol* 30: 2657–2670
- Brook RJ, Kingery WD (1967) Nickel ferrite thin films: microstructures and magnetic properties. *J Appl Phys* 38: 3589–3595



- Chen W, Zhu W, Ta OK, Chen XF (2010) Frequency and temperature dependent impedance spectroscopy of cobalt ferrite composite thick films. *J Appl Phys* 108:034101–034118
- Chinnasamy CN, Narayanasamy A, Ponpandian N, Chattopadhyay K, Shinoda K, Jeyadevan B, Tohji K, Nakatsuka K, Furubyashi T, Nakatani I (2001) Mixed spinel structure in nanocrystalline  $\text{NiFe}_2\text{O}_4$ . *Phys Rev B* 63:184108–184114
- Dutta S, Choudhary RNP, Sinha PK, Thakur AK (2004) Microstructural studies of  $(\text{PbLa})(\text{ZrTi})\text{O}_3$  ceramics using complex impedance spectroscopy. *J Appl Phys* 96:1607–1614
- Ghasemi A, Paesano A Jr, Machado CFC (2012) Structural and magnetic characteristics of  $\text{Co}_{1-x}\text{Ni}_{x/2}\text{Sr}_{x/2}\text{Fe}_2\text{O}_4$  nanoparticles. *J Magn Magn Mater* 324:2193–2198
- Gopalan VE, Malini KA, Saravanan S, Kumar DS, Yoshida Y, Anantharaman MR (2008) Evidence for polaron conduction in nanostructured manganese ferrite. *J Appl Phys D* 41:1–9
- Hafeli UO, Pauer GJ, Roberts WK, Humm JL, Macklis RM (1997) Scientific and clinical applications of magnetic carriers. Plenum Press, New York, p 501
- Hochepped JF, Bonville P, Pileni MP (2000) Nonstoichiometric zinc ferrite nanocrystals: syntheses and unusual magnetic properties. *J Phys Chem B* 104:905–912
- Idrees M, Nadeem M, Hassan MM (2010) Investigation of conduction and relaxation phenomena in  $\text{LaFe}_{0.9}\text{Ni}_{0.1}\text{O}_3$  by impedance spectroscopy. *J Phys D* 43:155401–155407
- Jacob J, Khadar MA (2010) Investigation of mixed spinel structure of nanostructured nickel ferrite. *J Appl Phys* 107:114310–114319
- Kodama RH, Berkowitz AE, McNiff EJ, Foner S (1996) Surface spin disorder in  $\text{NiFe}_2\text{O}_4$  nanoparticles. *Phys Rev Lett* 77:394–397
- Lee KS, Myung ST, Amine K, Yashiro H, Sun YK (2007) Structural and electrochemical properties of layered  $\text{Li}[\text{Ni}_{1-2x}\text{Co}_x\text{Mn}_x]\text{O}_2$  ( $x = 0.1–0.3$ ) positive electrode materials for lithium batteries. *J Electrochem Soc* 154:A971–A977
- Macdonald JR (1987) Impedance Spectroscopy. Wiley, New York ISBN 0471831220
- Macdonald JR (1992) Impedance spectroscopy. *Ann Biomed Eng* 20:289–305
- Mitchell DG (1997) MR imaging contrast agents—what's in a name? *J Magn Reson Imag* 7:1–4
- Morrison SA, Cahill CL, Carpenter EE, Calvin S, Swaminathan R, McHenry ME, Harris VG (2004) Magnetic and structural properties of nickel zinc ferrite nanoparticles synthesized at room temperature. *J Appl Phys* 95:6392
- Ortega N, Kumar A, Bhattacharya P, Majumder SB, Katiyar RS (2008) Impedance spectroscopy of multiferroic  $\text{PbZr}_x\text{Ti}_{1-x}\text{O}_3/\text{CoFe}_2\text{O}_4$  layered thin films. *Phys Rev B* 77:014111–014121
- Patange SM, Shirsath SE, Toksha BG, Jadhav SS, Jadhav KM (2009) Electrical and magnetic properties of  $\text{Cr}^{3+}$  substituted nanocrystalline nickel ferrite. *J Appl Phys* 106:023914–023921
- Phadatare MR, Khot VM, Salunkhe AB, Thorat ND, Pawar SH (2012) Studies on polyethylene glycol coating on  $\text{NiFe}_2\text{O}_4$  nanoparticles for biomedical applications. *J Magn Magn Mater* 324:770–772
- Son S, Taheri M, Carpenter E, Harris VG, McHenry ME (2002) Synthesis of ferrite and nickel ferrite nanoparticles using radio-frequency thermal plasma torch. *J Appl Phys* 91:7589–7591
- Srivastava A, Barg A, Morrison FD (2009) Impedance spectroscopy studies on polycrystalline  $\text{BiFeO}_3$  thin films on Pt/Si substrates. *J Appl Phys* 105:054103–054109
- Sugimoto M (1999) The past, present and future of ferrites. *J Am Ceram Soc* 82:269–280
- Suryavanshi SS, Patil RS, Patil SA, Sawant SR (1991) D.C. conductivity and dielectric behavior of  $\text{Ti}^{4+}$  substituted Mg-Zn ferrites. *J Less Comm Mater* 168:168–169
- Suryavanshi SS, Deshpand V, Sawant SR (1999) The effect of Mn and Al contents on the solvus of  $\kappa$  phase in austenitic Fe–Mn–Al–C alloys. *J Mater Chem Phys* 59:96–99
- Thakur A, Thakur P, Hsu J (2012) Magnetic behaviour of  $\text{Ni}_{0.4}\text{Zn}_{0.6}\text{Co}_{0.1}\text{Fe}_{1.9}\text{O}_4$  spinel nano-ferrite. *J Appl Phys* 111:07A305
- Tug LD, Kolesnichenko V, Caruntu G, Caruntu D, Remond Y, Golub VO, O'Connor CJ, Spinu L (2002) Annealing effects on the magnetic properties of nanocrystalline zinc ferrite. *Phys B* 319:116–121
- Waldron RD (1955) Infrared spectra of ferrites. *Phys Rev* 99:1727–1735
- Willard MA, Kurihara LK, Carpenter EE, Calvin S, Harris VG (2004) Chemically prepared magnetic nanoparticles. *Int Mater Rev* 49:125
- Wilson E, Wells AJ (1946) *J Chem Phys* 14:578
- Zaki HM, Mansour SF (2006) X-ray and IR analysis of Cu–Si ferrite. *J Phys Chem Sol* 67:1643–1648